Article:
Balakrishnan, Preethi Bala, Silvestri, Niccolò, Fernandez-Cabada, Tamara et al. (2020) Exploiting Unique Alignment of Cobalt Ferrite Nanoparticles, Mild Hyperthermia, and Controlled Intrinsic Cobalt Toxicity for Cancer Therapy. Advanced Materials. 2003712. ISSN: 0935-9648

https://doi.org/10.1002/adma.202003712

ADVANCED MATERIALS
www.advmat.de

Exploiting Unique Alignment of Cobalt Ferrite Nanoparticles, Mild Hyperthermia, and Controlled Intrinsic Cobalt Toxicity for Cancer Therapy

Preethi Bala Balakrishnan, Niccolò Silvestri, Tamara Fernandez-Cabada, Federica Marinaro, Soraia Fernandes, Sergio Fiorito, Mario Miscuglio, David Serantes, Sergiu Ruta, Karen Livesey, Ondrej Hovorka, Roy Chantrell, and Teresa Pellegrino**

Nanoparticle-based magnetic hyperthermia is a well-known thermal therapy platform studied to treat solid tumors, but its use for monotherapy is limited due to incomplete tumor eradication at hyperthermia temperature (45 °C). It is often combined with chemotherapy for obtaining a more effective therapeutic outcome. Cubic-shaped cobalt ferrite nanoparticles (Co–Fe NCs) serve as magnetic hyperthermia agents and as a cytotoxic agent due to the known cobalt ion toxicity, allowing the achievement of both heat and cytotoxic effects from a single platform. In addition to this advantage, Co–Fe NCs have the unique ability to form growing chains under an alternating magnetic field (AMF). This unique chain formation, along with the mild hyperthermia and intrinsic cobalt toxicity, leads to complete tumor regression and improved overall survival in an in vivo murine xenograft model, all under clinically approved AMF conditions. Numerical calculations identify magnetic anisotropy as the main Co–Fe NCs' feature to generate such chain formations. This novel combination therapy can improve the effects of magnetic hyperthermia, inaugurating investigation of mechanical behaviors of nanoparticles under AMF, as a new avenue for cancer therapy.

Oncothermia is a type of cancer therapy that utilizes heat to suppress tumors. Magnetic nanoparticles (MNPs) can convert electromagnetic energy to heat energy in the presence of an alternating magnetic field (AMF). Most of the studies from the last two decades investigating in vivo oncothermia comprise biocompatible and biodegradable iron oxide-based nanoplatforms. Currently, the only clinically approved magnetic hyperthermia (HT) therapy employs spherical aminosilane coated iron oxide nanoparticles (IONPs, namely, NanoTherm MagForce Nanotechnologies) to treat glioblastoma multiforme in patients and currently in clinical trial for prostate cancer.[1] The major drawback of this system is that it requires a very high concentration of IONPs to achieve the temperature needed to kill cancer cells (43–45 °C). This is mainly due to their low specific absorption rate (SAR) value, which is a direct measure of the heating capacity of the MNPs under AMF.

Cubic-shaped IONPs (IONCs) represent by far the benchmark product available with SAR values higher than spherical IONPs specifically due to their particular cubic shape and anisotropy.[2–4] Furthermore, to improve the

Dr. P. B. Balakrishnan,[+] Dr. N. Silvestri, Dr. T. Fernandez-Cabada, Dr. F. Marinaro,[++] Dr. S. Fernandes,[+++] Dr. S. Fiorito, Dr. M. Miscuglio,[++++] Dr. T. Pellegrino
Istituto Italiano di Tecnologia
Via Morego 30, 16163 Genova, Italy
E-mail: teresa.pellegrino@iit.it

The ORCID identification number(s) for the author(s) of this article can be found under https://doi.org/10.1002/adma.202003712.

[+]Present address: The George Washington Cancer Center, The George Washington University, 800 22nd St NW, Washington, DC 20052, USA
[++]Present address: Department of Cancer and Developmental Biology & Zayed Center for Research into Rare Disease in Children, UCL Great Ormond Street, Institute of Child Health, 30 Guilford Street, London WC1N 1EH, UK
[+++]Present address: International Clinical Research Center (ICRC) of St Anne's University Hospital, CZ-65691 Brno, Czech Republic
[++++]Present address: Department of Electrical and Computer Engineering, The George Washington University, 800 22nd St NW, Washington, DC 20052, USA

Dr. D. Serantes
Instituto de Investigacións Tecnolóxicas and Departamento de Física Aplicada
Universidade de Santiago de Compostela
Santiago de Compostela 15782, Spain
E-mail: david.serantes@usc.gal

Dr. S. Ruta, Prof. R. Chantrell
Department of Physics
University of York
York YO10 5DD, UK

Dr. K. Livesey
UCCS Biofrontiers Center and Department of Physics
University of Colorado at Colorado Springs
Colorado Springs, CO 80918, USA

Dr. O. Hovorka
School of Engineering and Physical Sciences
University of Southampton
Southampton SO16 7QF, UK

DOI: 10.1002/adma.202003712

heating capacity of these well exploited spherical or cubic shaped IONPs, researchers have completely or partially replaced, the iron moiety (Fe^{2+}) with other ions including cobalt (Co^{2+}), nickel (Ni^{2+}), manganese (Mn^{2+}), and zinc (Zn^{2+}) leading to exploration of these spinel ferrites.[4–6] It was determined that the resulting spinel ferrites have tunable SAR values, somewhat better than IONPs due to their larger coercivity values and wider hysteresis loop, which directly translates into the production of more heat under AMF.[7] Additionally, despite the success stories of IONP-based HT, it is often shown that, the effect of heat produced under HT alone is not sufficient to achieve complete tumor suppression. HT is often combined with other therapies and most commonly with chemotherapies.[8] This is also the case in the clinical study discussed earlier, where the IONP-based HT was followed by radiotherapy or chemotherapy.[1] We have previously investigated this combination, IONC-based HT and chemotherapy utilizing doxorubicin.[9,10]

Among the mixed ferrites, cobalt ferrite nanoparticles (Co–Fe NPs), despite their high coercivity value about one order of magnitude larger than that of IONPs, are the least exploited material in biological studies, due to its well-documented toxicity profile given by the degrading cobalt ions.[11] In fact, only a handful of preclinical studies are available to date that demonstrate the use of Co–Fe NPs as hyperthermia agent for cancer therapy.[12,13] In most in vivo studies, the Co–Fe NPs were exploited as diagnostic tools pertaining to their outstanding T2 relaxivity traces in magnetic resonance imaging (MRI).[14,15] The well-established intrinsic toxicity of Co ions can be converted into a useful tool representing a cytotoxic agent acting similar to chemotherapeutic agent, by simply controlling the etching and the release of the Co from the MNP surface. The uptaken cobalt ferrite nanoparticles can undergo degradation within lysosome, at acidic pH, leading to slow etching and release of the included cobalt ions.[16,17] In fact, heavy metals and toxic elements are already in use in clinical chemotherapy.[18] Instead of using a separate cytotoxic agent, the use of Co–Fe NPs could potentiate delivery of toxic Co ions, as a form of chemotherapy to tumor cells.[19]

Motivated by these ideas, in this study, we aimed to demonstrate the use of cubic-shaped cobalt ferrite nanoparticles (Co–Fe NCs) to exploit the dual therapy utilizing the heat produced by Co–Fe NCs in the AMF and the intrinsic toxic effects of Co ions released from the NPs following slow degradation in tumor microenvironment, for improved cancer therapy. We utilized Co–Fe NCs with cubic edge size of 17 nm and compared it both in vitro and in vivo, with standard IONCs for efficacy in heat production and tumor suppression. We also investigated the long-term survival of the Co–Fe NCs in treated animals and profiled the biodegradation of the injected Co–Fe NCs in xenograft tumor model utilizing nude mice with A431 human epidermoid carcinoma. Despite a moderate heat temperature at the tumor and the expected cobalt cytotoxicity, we found that the Co–Fe NCs formed long chains comprising multiple nanocubes at the tumor site. The length of these chains increased under HT treatment. On the contrary, the IONCs did not form the nanoparticle chains under similar HT treatment conditions and failed to reduce tumor mass. This discrepancy in chain formation between the two nanocubes was further predicted by numerical calculations based on simple physical observations. In short, this article focuses on three considerations: two well-known behaviors of Co–Fe NCs, namely: 1) mild hyperthermia causing local heat damage and 2) the associated local intrinsic cobalt toxicity that can be controlled by site-specific intratumoral injections and lastly a very unique property of Co–Fe NCs, and 3) the chain formation that can be increased upon HT. We propose this triple chemo-magnetomechanical heat damage therapy as novel multimodal therapy for cancer treatment.

In detail, cubic-shaped cobalt ferrite nanoparticles of stoichiometry $Co_{0.65}Fe_{2.35}O_4$ (Co–Fe NCs) were prepared by a thermal-decomposition method and coated with poly(maleic anhydride-*alt*-1-octadecene)(PMAO) to render them water-soluble and usable for biological applications, following well-established procedures developed in our laboratory (**Figure 1**a).[5,20] The transmission electron microscopy (TEM) images of water transferred Co–Fe NCs showed monodispersed particles with mean edge size of 17 ± 2 nm (Figure 1b; Figure S1, Supporting Information). The hydrodynamic size measured by DLS was 47 nm (0.08 PDI) indicating a uniform size distribution (Figure S2, Supporting Information). In order to compare the hyperthermia performance of the Co–Fe NCs coated with PMAO, standard IONCs of similar size (17 ± 2 nm) were prepared and coated with the same polymer (Figure 1c).[3] To compare the heating efficiency of these nanocubes under AMF, SAR measurements were conducted at various frequencies (*f*: 105, 220, and 300 kHz) and field (*H*: 12, 16, 20, and 24 kA m^{-1}) conditions. The SAR values of IONCs in aqueous solutions was comparatively higher than Co–Fe NCs at frequencies of 220 and 300 kHz, but at lower frequency conditions (105 kHz and 20 kA m^{-1}), the SAR of Co–Fe NCs was 400 W g^{-1}, which was twice higher than IONCs (200 W g^{-1}; Figure 1d) within the biologically acceptable AMF limits ($H \cdot f$ value: 5×10^9 kA m^{-1} Hz^{-1}).[21]

The complex dependence of SAR on frequency and field is mainly due to the large difference in the effective anisotropy between both particle types (discussed in detail later). For the small-anisotropy IONCs, increasing the frequency leads to the development of a larger number of nanoparticles showing hysteresis and therefore increases hysteresis losses and the SAR; one can see this behavior in Figure 1d at all maximum field values investigated. On the other hand, the SAR of the high-anisotropy Co–Fe NCs is strongly field dependent and weakly dependent on the frequency. It seems likely that this arises because the Co–Fe NC system is in the regime of minor hysteresis loops in small fields. In this regime, increasing frequency is compensated by a decrease in the area of the hysteresis loop, resulting in a weak frequency dependence. Increasing the field will have the strong effect of moving the system toward full hysteresis, which consequently increases the SAR, consistent with the behavior shown in Figure 1d.

In vitro cytotoxicity of Co–Fe NCs was assessed using A431 epidermoid carcinoma cells. The cells were exposed to two different concentrations of Co–Fe NCs (25×10^{-9} and 50×10^{-9} M) and compared to the cytotoxicity of IONCs of same size, surface coating, and concentration. While both concentrations of IONCs showed no toxicity up to 72 h, the Co–Fe NCs began to exhibit mild toxicity at 24 h, which gradually increased for 72 h: 25% toxicity for 25×10^{-9} M of Co–Fe NCs, and a 50% toxicity (lethal dose 50, LD50) for 50×10^{-9} M Co–Fe NCs (Figure 1e). As expected, this confirms the toxic profile of polymer coated Co–Fe NCs compared to nontoxic IONCs, which proves that the toxicity is more likely due to the

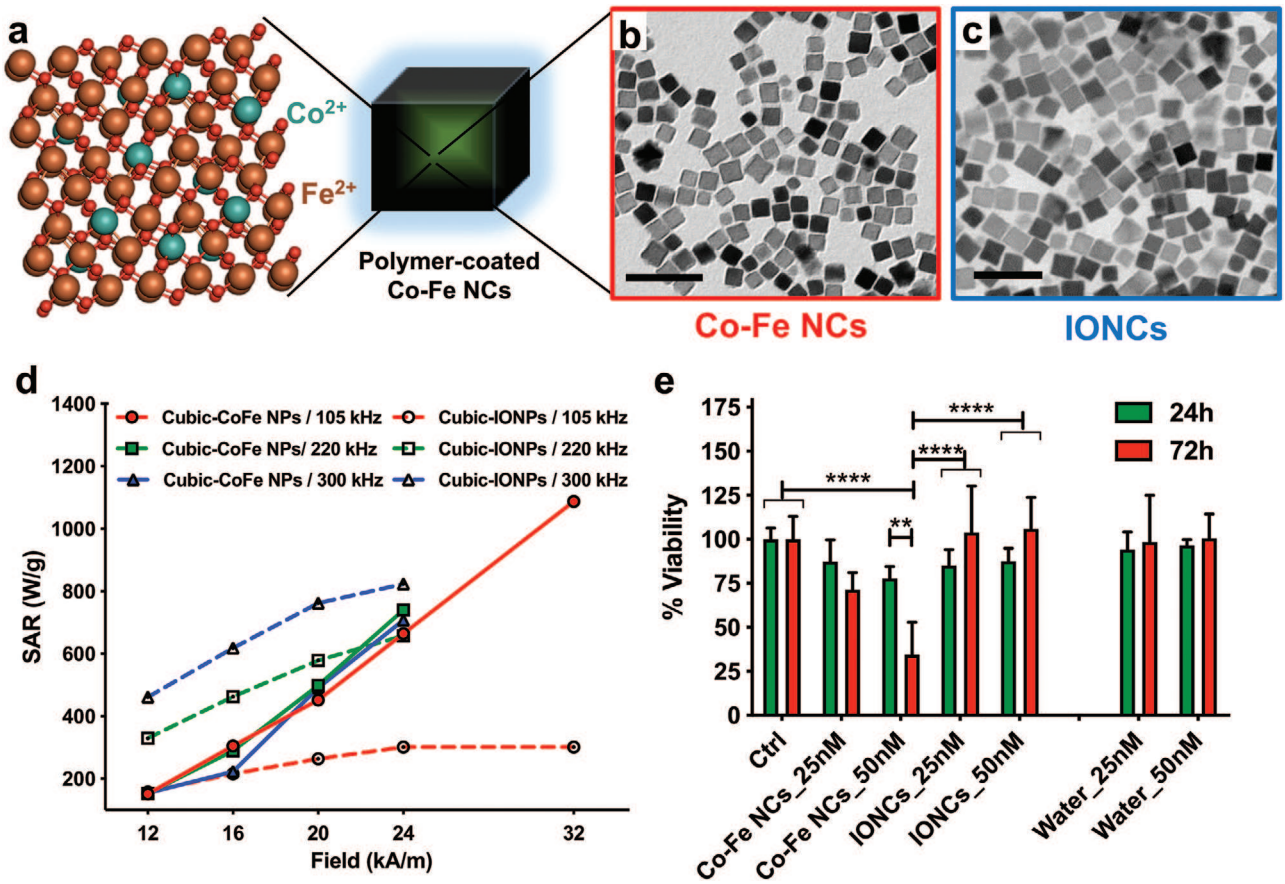

Figure 1. Characterization of cobalt ferrite nanocubes. a) A schematic representation of aqueous solution of poly(maleic anhydride-*alt*-1-octadecene) (PMAO) polymer-coated Co–Fe NCs compatible for biological application. b,c) TEM images of PMAO-coated Co–Fe NCs with mean sizes of 17 ± 2 nm (b) and PMAO-coated IONCs with mean sizes of 17 ± 2 nm showing a monolayer carpet of nanoparticles and the absence of aggregates (c). Scale bar represents 50 nm. d) SAR measurements at different field intensities (12, 16, 20, 24, and 32 kA m^{-1}) and frequencies (105, 220, and 300 kHz), showing higher SAR value for Co–Fe NCs at lower clinically relevant AMF conditions (105 kHz and 20 kA m^{-1}) compared to IONCs. e) LDH cytotoxicity assay showing no toxicity for IONCs and significant intrinsic toxicity of Co–Fe NCs on A431 epidermoid carcinoma cells at 25×10^{-9} and 50×10^{-9} M concentrations.

Co ions in the Co–Fe NCs and not due to the size, shape, or the iron (Fe) moiety of the nanocubes.[22]

In the first in vivo efficacy study, we aimed to understand the heating efficiency of the Co–Fe NCs to function as hyperthermia agents in a murine xenograft tumor model using nude mice and human A431 epidermoid carcinoma cells. Polymer-coated Co–Fe NCs ([Co+Fe] = 0.7 mg) were injected intratumorally (i.t.) in the palpable tumor developed in the flank of the mice. I.t. injection was chosen in order to localize the toxicity of Co–Fe NCs and evaluate the HT efficacy with respect to IONCs (0.7 mg of Fe). The gallic acid PEG coated IONCs used as comparative standard in this study has been previously investigated by our laboratory for its superior HT performance both in vitro and in vivo.[10] Given the high SAR value of the Co–Fe NCs under clinical HT conditions (105 kHz and 24 kA m^{-1}; Figure 1c), we have chosen to use these alternating magnetic field parameters for all in vivo studies hereafter (**Figure 2**a). In short, NPs were injected when the tumors were ≈80–100 mm^3 (day 0), followed by 30 min HT cycles on day 0, day 1, and day 2, totaling 3× HT cycles on three consecutive days (HT1, HT2, and HT3). During the course of the 3× HT treatments, for animals i.t. injected with IONPs (TEM; Figure 2b) or Co–Fe NCs (TEM; Figure 2c), the temperature of the tumor (T_{Tumor}) and the temperature of the skin of the tail (away from tumor, T_{Skin}) was monitored using an IR camera (Figure 2d). The difference between the temperature of the tumor and of the skin ($\Delta T = T_{Tumor} - T_{Skin}$) was found to be about 6 °C for IONCs on HT1, but this decreased to about 3.5 °C on HT2 and HT3. On the contrary, Co–Fe NCs showed a ΔT of only 3 °C on HT1, but this value was maintained at HT2 and HT3. The observed reduced temperature and in turn SAR performances, for Co–Fe NCs with respect to the same Co–Fe NCs in water media (Figure 1d) could be due to immobilization of the nanocubes in the viscous tumor/environment or to the strong interparticle interactions within the cellular environment (as also discussed later)[23], as it is known that interparticle interactions diminish the heat release of high anisotropy particles.[24]

Despite the unlikely prospect to reach the desired higher temperature using the Co–Fe NCs, tumor growth was monitored for 12 days after treatment initiation. The Co–Fe NCs with HT (Co–Fe NCs + HT) help delay the tumor growth, although the tumor reducing property compared to its non-HT counterpart (Co–Fe NCs) or the IONCs with and without HT (IONCs and IONCs + HT, respectively) was not significant (Figure 2f). The results

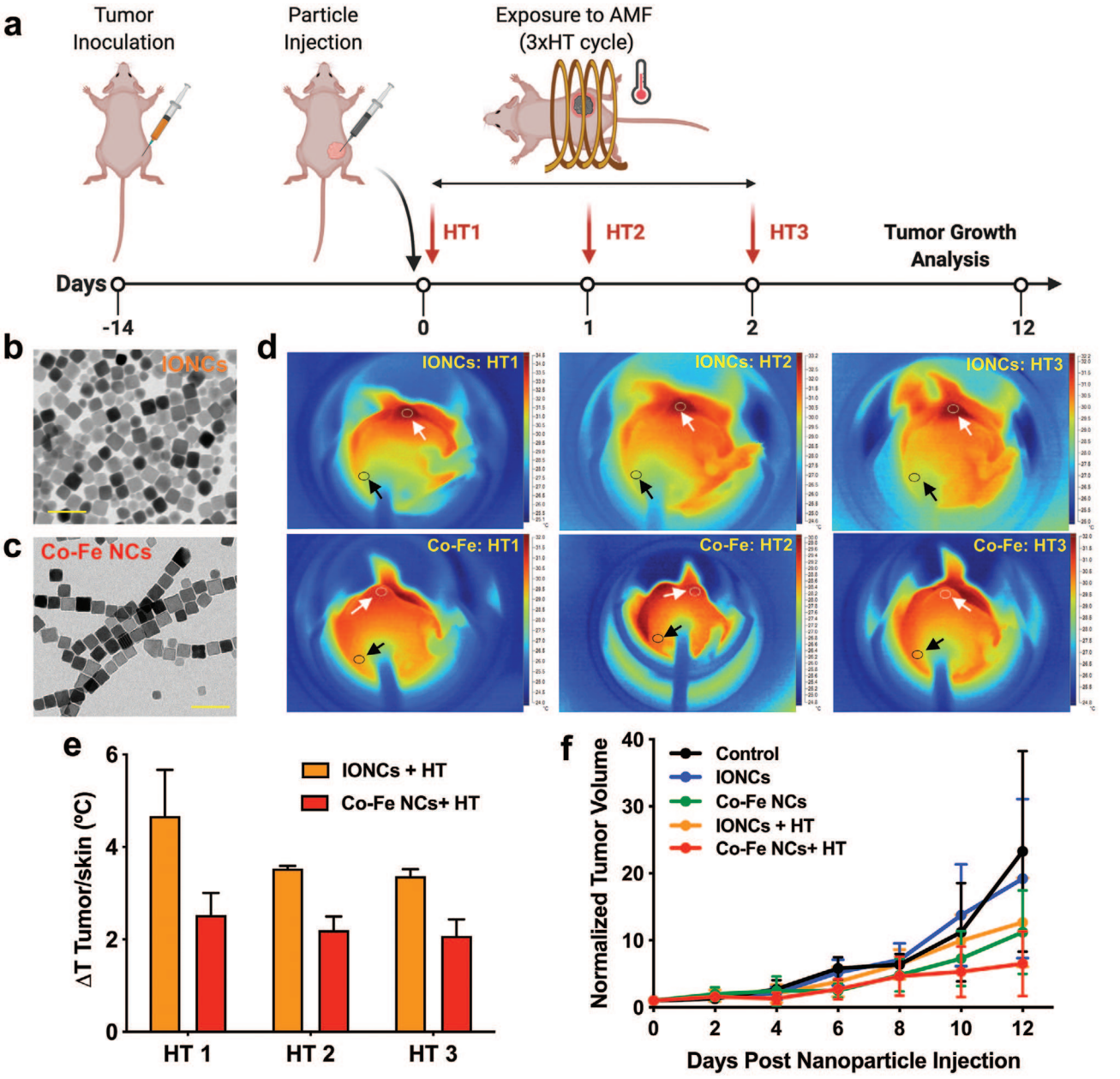

Figure 2. Comparison of in vivo efficacy of Co–Fe NC and IONC-based hyperthermia. a) Schematic timeline representation of the treatment strategy. The black arrow represents particle injection (0.7 mg Co–Fe NCs or 0.7 mg IONCs) and the red arrows represent days of HT treatments (3× HT) using clinically acceptable AMF conditions (*f*: 110 kHz; *H*: 20 kA m^{-1}). b,c) TEM images of ligand-exchanged IONCs with mean sizes of 18 ± 3 nm (b) and PMAO-coated Co–Fe NCs with mean sizes of 17 ± 2 nm (c) used for the in vivo experiments. Scale bar represents 50 nm. d) Infrared images of a mouse injected with IONCs and Co–Fe NCs during HT treatment at day 1 (HT1), day 2 (HT2), and day 3 (HT3). The white and black arrows highlight the temperature at tumor and the skin respectively, utilized to generate Δ*T* values. e) Δ*T* graph ($\Delta T = T_{Tumor} - T_{Skin}$) plotted for HT1, HT2, and HT3 for animals injected with IONCs (orange bars) or Co–Fe NCs (red bars). f) Tumor growth curve showing the marginal reduction in tumor growth for animals injected with Co–Fe NCs and subjected to 3× HT (Co–Fe NCs + HT) compared to the other groups studied (Control, Co–Fe NCs alone, IONCs alone, and IONCs + HT). $N = 6$.

obtained with respect to IONCs + HT are comparable with previously reported in vivo study.[10] Importantly, an effective tumor reduction was never achieved when 18 nm IONP-based hyperthermia alone was used as a monotherapy platform.[10] Instead, intravenous injection of doxorubicin (combination therapy: IONCs + HT + Doxo) was required to increase the efficacy of IONC-based HT.[9]

Given the rather low heating profile associated with Co–Fe NCs under HT treatment, and the marginal improvement in delaying tumor growth, we proceeded to further investigate the reason behind this inconsistency. TEM images of the treated tumors at day 12 post-injections were analyzed to study the effect of HT within the ultrastructures of the cell. TEM images of both IONCs (**Figure 3**a,b) and Co–Fe NCs (Figure 3c,d) show

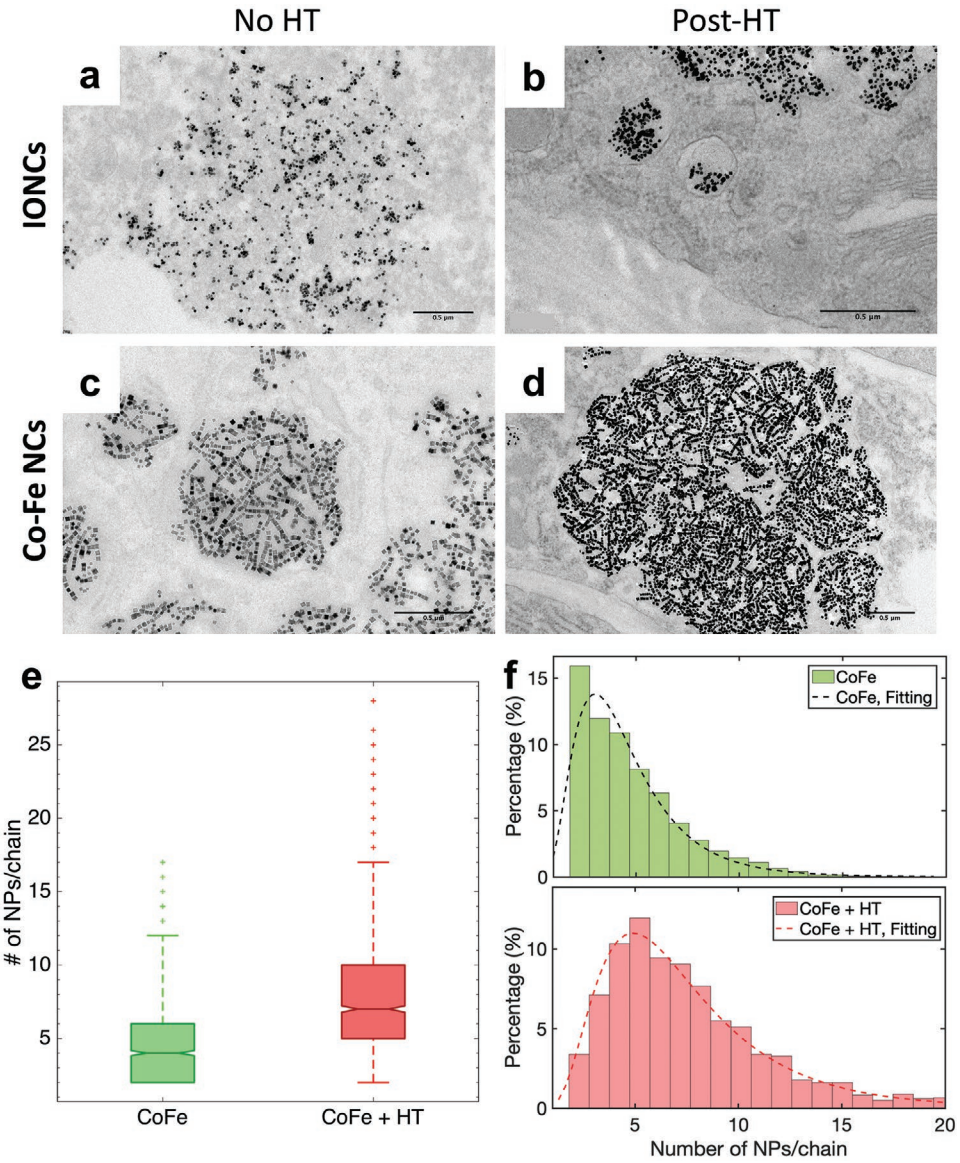

Figure 3. Investigation of the chain formation of cubic shape Co–Fe NPs in vivo. a–d) Transmission electron microscopy images of tumors injected with IONCs (a,b) and Co–Fe NCs (c,d). Tumors injected with IONCs did not show any specific NP arrangements without (a) or with (b) HT. Chain-like structures were evident in tumors injected with both Co–Fe NCs alone (c) and Co–Fe NCs + HT (d). All images represent analysis on tumors 12 days post-treatment and the scale bar represents 0.5 µm. e,f) MATLAB was used to determine the number of particles per chain in TEM images of Co–Fe NCs and Co–Fe NCs + HT. e) Notched box plot distribution of the number of NPs per chain in the Co–Fe NCs alone and the Co–Fe NCs + HT group highlighting a greater number of NPs per chain for the Co–Fe NCs + HT than its non-HT counterpart. Histogram showing the distribution of the number of NPs per chain in the Co–Fe NCs (green bars) and Co–Fe NCs + HT (red bars). The entire range is divided into bins of one nanocube width. f) The dashed line in the graph represents the log-normal distribution function that fits the population of the two groups being studied, showing HT treatment favors the addition of further nanocubes to the already existing chains at the tumor.

presence of these nanoparticles within well-defined endosomal structures. This localization can potentially promote degradation of these nanocubes at acidic endosomal pH, particularly in the case of Co–Fe NCs releasing toxic cobalt within the tumor cells, leading to their destruction.[16,17] Also, the groups treated with IONCs and IONCs + HT did not show any unique alignment of nanocubes (Figure 3a,b). Unexpectedly the Co–Fe NCs structures found within the tumors, both with and without HT, were forming chain-like alignments (Figure 3c,d). To quantify the chain formation, we analyzed the TEM images and determined the number of particles per chain in Co–Fe NCs and Co–Fe NCs + HT tissue samples using a MATLAB program. The percentage of different number of chains formed per each group was determined and fitted using a log-normal distribution. Notched box plot distributions of the number of nanocubes per chain (NCs/chain) in the Co–Fe NCs alone and the Co–Fe NCs + HT showed increased number of NCs/chain for the latter than its non-HT counterpart. The Co–Fe NCs chains have a median of 4 NCs/chain and this distribution shifted to 7 NCs/chain after HT (Figure 3e), proving that

HT increases the number of nanoparticles in the chain. Also, this statement is further reinforced by the histograms showing the distribution of the NCs/chain in the Co–Fe NCs (green bars) and Co–Fe NCs + HT (red bars). The mode value (highest repeating number of cubes per chain) of the log-normal distribution was 3.01 (3 cubes) for Co–Fe NCs and 4.9 (5 cubes) for Co–Fe NCs + HT (Figure 3f). Overall, the chains in the samples treated with HT had an augmented chain length (a 1.62-fold increase) with respect to the non-HT treated samples.

To determine if the chain length increase occurred immediately after the first 30 min of HT in the tumor, we emulated the in vivo HT setup in vitro using different % of glycerol or Matrigel, simulating a tumor-like environment (phantom) (Figures S3 and S4, Supporting Information). TEM images of the matrigel phantom clearly indicated the presence of chains after just one cycle of HT (Figure S4, Supporting Information). To the best of our knowledge, while the formation of chains has been reported in quite a few in vitro studies conducted in test tube setup containing the Co–Fe NPs, it has never been observed or reported in in vivo conditions at the tumor site, especially demonstrating increase in chain length post-HT under AMF.[19]

To understand if the chain formation is magnetically feasible under our experimental conditions for Co–Fe NCs (17 ± 2 nm) and is less feasible for IONCs of approximately similar cube edge (18 ± 3 nm), we have developed the following qualitative arguments. Namely, we consider the NP size dependence of the Néel and Brownian relaxation times, which are the main characteristic timescales determining the physical behavior of Co–Fe NCs and IONCs under a time-varying magnetic field. Néel relaxation relates to thermal fluctuations of magnetic moments of NPs and the corresponding Néel characteristic time is[25]

$$\tau_N = \frac{\sqrt{\pi}}{A}\tau_0 \frac{e^{\Gamma}}{\Gamma^{1/2}} \quad (1)$$

where $\tau_0 = 1$ ns is the attempt time, $A = 2$ and $\Gamma = KV/k_BT$ (the ratio of anisotropy energy to thermal energy) for NPs with uniaxial magnetocrystalline anisotropy, and $A = 4$ and $\Gamma = K_1V/4k_BT$ for NPs with cubic anisotropy. To a good approximation, the anisotropy is assumed to be uniaxial for IONCs with its value estimated as $K = 1.1 \times 10^5$ erg cm^{-3} (Figures S5 and S6, Supporting information) and cubic for Co–Fe NCs with $K_1 = 2 \times 10^6$ erg cm^{-3}. Brownian relaxation relates to positional rotational and translational fluctuations of NPs with the rotational (τ_B) and translational (diffusion, τ_{diff}) relaxation times defined as

$$\tau_B = \frac{3\eta V_{hyd}}{k_BT} \quad (2)$$

$$\tau_{diff} = \frac{\chi^2 6\pi\eta R_{hyd}}{k_BT} \quad (3)$$

where η is the viscosity of the embedding medium, V_{hyd} and R_{hyd} are the hydrodynamic volume and diameter, respectively, and χ is the characteristic diffusion length (see Equation (S4) in the Experimental Section in the Supporting Information).

It is apparent that the formation of stable magnetic chains is expected when $\tau_N \gg \tau_B, \tau_{diff}$. This is because only under this condition the magnetic moments of NPs remain stable on the timescales of Brownian fluctuations and magnetic dipolar interaction between the nanocubes can sufficiently prevail and drive the physical assembly of nanocubes into chains. Therefore, in the following, we identify the parameter region where the τ_N dominates τ_B and τ_{diff}.

This is demonstrated in the bottom panel of **Figure 4**, which shows the dependence of these relaxation times versus the nanocube size and illustrates considerably different locations and slopes of the τ_N curves for Co–Fe NCs and IONCs. Namely, for Co–Fe NCs the τ_N becomes dominant for smaller nanocube edge size (≈12 nm) than for the IONCs (≈18 nm), and clearly this difference is to be attributed to different magnitudes of the magnetocrystalline anisotropy of these NPs. Moreover, when the experimental size distributions of NPs are taken into consideration in the analysis (Figure 4, top), it becomes evident that while only 42% of IONCs are expected to be within the chaining region, i.e., the size region with dominant τ_N, and thus have the possibility to form chains, for Co–Fe NCs the whole NPs size distribution (100%) lies within the aggregation region. This shows that the likelihood of observing chaining for Co–Fe NCs is indeed significantly higher than for the IONCs, which corroborates our experimental observations.

The problem of chaining in magnetic nanoparticle systems has generally been investigated for spherical rather than cubic nanoparticles.[26] However, simple theoretical estimates can

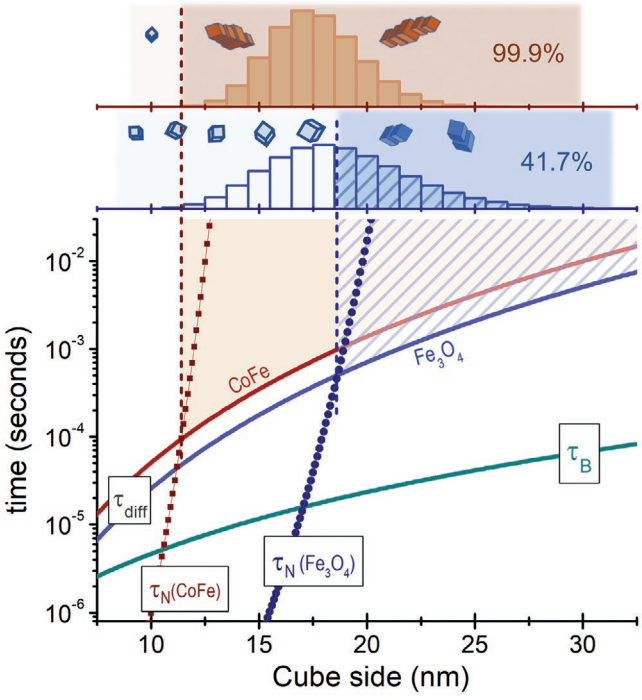

Figure 4. Bottom: Identifying the active part of the particle size distribution, where the Néel relaxation time (τ_N, dotted lines) is longer than the Brownian translational and rotational relaxation times (τ_{diff} and τ_B, respectively, solid lines) of particles, in order to gauge the likelihood of chain formation for IONCs (Fe_3O_4: blue) and Co–Fe NCs (CoFe: brown). The relaxation times were calculated using Equations (1)–(3). Top: fractions of the IONCs (42%) and Co–Fe NCs (100%) size distributions susceptible to chain formation.

provide an initial insight into the relative likelihood of spherical and cubic particles to form chains. This is based on the usual parameter for estimation of magnetic coupling strength, $\lambda = \mu_0 (M_s V)^2/(2\pi d_{cc}^3 k_B T)$, where M_S and V are the saturation magnetization and particle volume, respectively, and d_{cc} is the center-to-center interparticle separation distance. Considering that the interparticle distance is equal to the side L = 17 nm plus twice the 2 nm thickness coating for the cubes, and for the sphere the particle diameter ($d \approx 21$ nm derived by considering a spherical nanoparticle of the same volume of a nanocube particle of 17 nm in cube edge) plus again twice the particle coating thickness, it is readily obtained that the spherical geometry results in significant reduction of the coupling strength, of about 41%. Thus, for particles of the same size, spherical shape appears less favorable for chain formation.

We can also comment on the fact that longer Co–Fe NC chains are observed upon the exposure to alternating magnetic field. First, we observe in our experiments random chain orientation with no apparent tendency toward a preferential alignment along the applied field direction. One feasible way the chains can increase their average length is through the action of stray dipolar magnetic fields emanating from the already formed chains. Subjecting such chains to an applied magnetic field results, on average, in their increased thermal stability, especially for chains oriented away from the perpendicular direction with respect to the applied field. The increased thermal stability enhances the stray dipolar fields, thereby increasing the likelihood of attracting additional particles toward the ends of the chains. Note that this effect is expected to be the strongest for chains oriented along the applied field. The second and more subtle effect that may lead to chain growth can result from the (moderate hyperthermic) temperature increase of the environment. Such a temperature increase will enhance the Brownian diffusion of NPs, thereby increasing the likelihood of NP attraction toward the chains and promoting the increase in chain length. Although the temperature increase will also lead to reduced thermal stability of chains, this effect is less dominant as demonstrated in Figure S7 in the Supporting Information.

Having observed the presence of chains only for Co–Fe NCs, a long-term in vivo study was conducted following the same experimental scheme utilized earlier, to verify the persistence of chain formations and the prolonged cobalt toxicity, which could produce tumor reduction and longer survival (**Figure 5**a). For this study, we focused only on the efficacy of Co–Fe NCs with or without HT. Consistent with our previous observations, the HT treatments increased temperature at the tumor site by few degrees (IR images in Figure S8 in the Supporting Information). Digital photographs taken on day 0 and day 15 for control animals show an increase in tumor size, whereas Co–Fe NCs treatment reduced tumor size and Co–Fe NCs + HT treatment completely suppressed the tumor by day 30 (Figure 5b). I.t. injection of Co–Fe NCs alone significantly delayed the growth of tumors compared to untreated animals (Control), but this was not sufficient to completely eradicate tumor growth, as indicated by slow but gradual increase of tumor volume after 30 days. Instead, tumors treated with Co–Fe NCs followed by 3× HT (Co–Fe NCs + HT) showed tumor reduction within 30 days with no tumor recurrence up to 200 days post-treatment (Figure 5c). In addition, for the same Co–Fe NCs + HT group the survival rate was significantly higher than all the other groups studied, showing disease-free survival of up to 200 days (7 months). Meanwhile, the Control group and Co–Fe NCs group without the effects of HT succumb to disease much earlier with maximum survival rate of 22 and 30 days, respectively (Figure 5d).

Interestingly, TEM images of tumor tissues at day 30 consistently showed long chain formation (Figure 5e,f), indicating that the nanocube–nanocube interactions is strong and once formed, they persist for a longer period. The histopathological studies at day 30 conducted on the tumor tissue of animals treated with Co–Fe NCs (with or without HT) showed that the NPs were present inside the tumor, indicated by the Prussian blue staining (Figure 5g,h; Figure S9, Supporting Information). The Co–Fe NCs + HT group showed a swirling movement of nanocubes from the point of injection (center of the tumor) to the tumor periphery, a phenomenon previously observed due to the applied AMF (Figure 5h).[10] This data suggests that the injected Co–Fe NCs, already forming chains, could cause mechanical damage to the tissue while moving from the point of injection to the tumor periphery during the HT cycles (chain length increases with HT and can cause more damage). The presence of an almost impermeable outer viable collagenous layer at the tumor periphery is one of the main reasons that the tumor tissues thrive. While the growing tumor gets necrotic in the center, this outer layer containing viable cells and enriched angiogenesis at these sites, makes the tumor grow in volume. In addition, this thick layer and its tight arrangement of cellular architecture in a collagen rich environment protects the inner tumor cells from incoming drugs and other therapies.[27] In this case, the i.t. injection ensured that the particles were delivered in a controlled manner inside the tumor, minimizing nonspecific cobalt toxicity. Also, i.t. injection is an acceptable palliative care for cancer patients.[28] The outer collagen-rich layer of the Co–Fe NCs + HT (Figure 5h), which is indicated by a fast red stained collagen (darker pink) and cells (pink) in the outer layer, was almost completely absent (more toxicity at the periphery leading to stroma destruction), while it was still viable in case of the Co–Fe NCs alone (Figure 5g). This complete destruction of the outer tumor membrane could also contribute to the complete tumor reduction and lack of recurrence in the Co–Fe NCs + HT treated animals (Figure 5c).

A major concern when dealing with nanoparticles that contain a toxic element is the biodistribution profile. Among magnetic nanoparticles, the biodegradation profile of IONPs is among the most investigated HT agents.[29] Although few in vivo works on Co–Fe NPs of different size and shape than the one reported here, have shown successful tumor reduction, these studies failed to track the fate of these nanoparticles post-treatment completion.[13,14] To address this concern, we measured the elemental amount of Fe and Co in tumor (site of injection) and spleen. Indeed, a recent study showed that i.t. injected Co–Fe NPs can be tricked into being eliminated via the ferritins following the same method our body uses to eliminate the Fe ions through the spleen.[17] The tumor and spleen of treated animals were analyzed as and when they reached their endpoint and thus, we were able to track the fate of Co–Fe NCs from day 20 (shortest survival) up to day 80 (longest survival for tumor-bearing animal) post-HT using ICP-MS elemental analysis

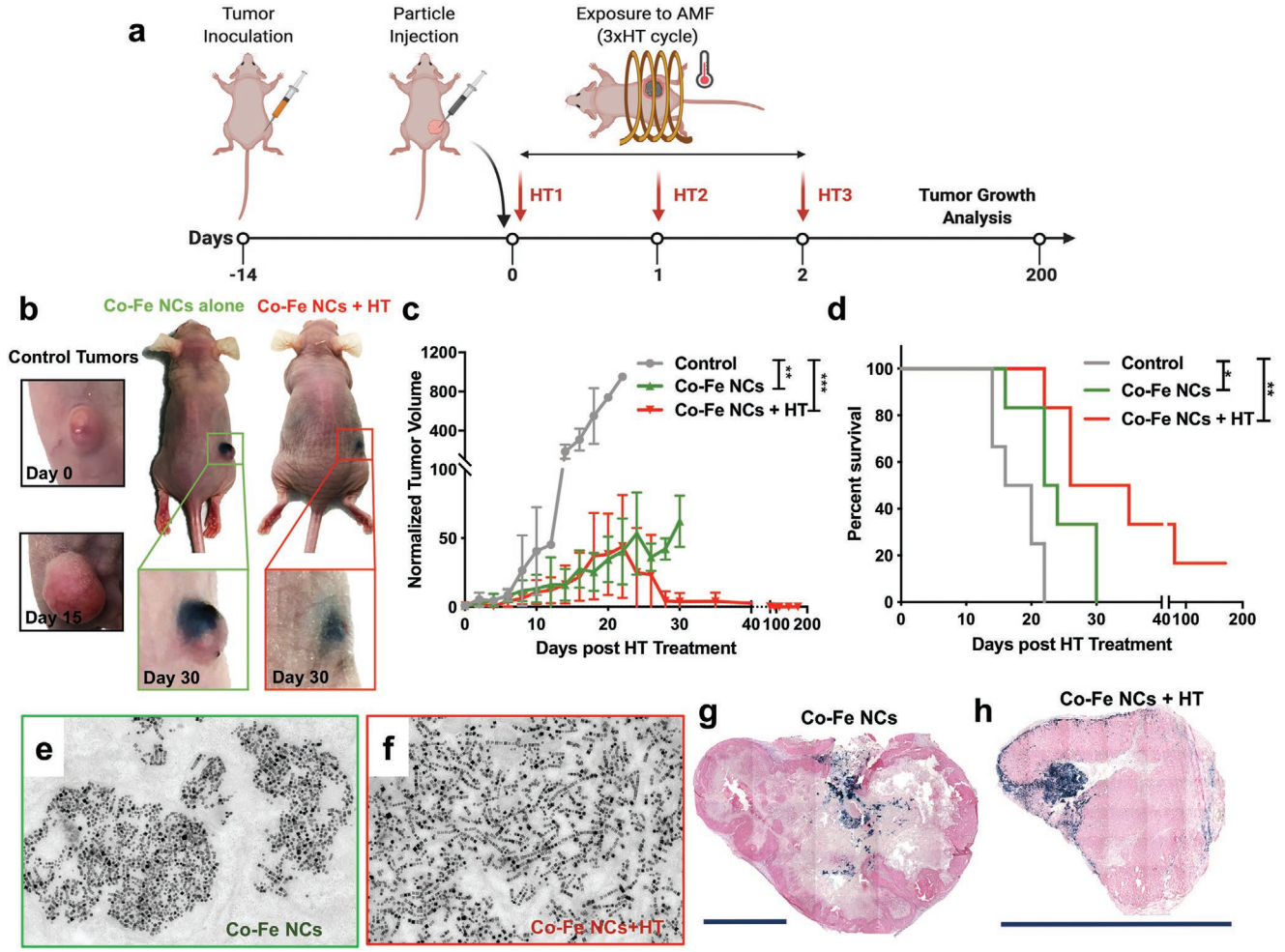

Figure 5. A long-term study of in vivo HT efficiency of Co–Fe NCs. a) Schematic timeline representation of the treatment strategy. b) Photographic comparison between the control, untreated animal (Control: day 0 and day 15) and the animal treated with Co–Fe NCs alone and Co–Fe NCs + HT, showing the reduction and complete elimination of the tumor 30 days post-treatment, respectively. The images in the boxes show enlarged image of the treated tumor. c) Tumor growth curve showing the complete elimination of the tumor, and no recurrence up to 200 days for animals treated with Co–Fe NCs + HT. d) A Kaplan–Meier survival plot demonstrating the highest survival rate for animals treated with Co–Fe NCs + HT for up to 200 days post-treatment compared to other groups with a maximum survival rate of up to only 30 days. e,f) TEM images of tumors injected with Co–Fe NCs proving persistent chain-like structures even at day 30 post-treatment for both Co–Fe NCs alone (e) and Co–Fe NCs + HT (f). g,h) Light microscopy images of tumor slices obtained from groups treated with Co–Fe NCs alone (g) and Co–Fe NCs + HT (h), showing the presence of the injected NPs and a complete absence of stroma in the latter case. The NPs are shown in blue using Prussian blue staining; collagen stained in dark-pink and cells in light-pink due to Fast Red staining. Scale bars in (g) and (h) represent 0.5 cm.

(**Figure 6**). The tumors and spleens showed different levels of both Fe and Co depending on days following the treatment. It is interesting to notice the reduction in Fe levels in tumor over days and subsequent increase of the same in spleen, indicating the elimination of Fe from injected site (Figure 6a,c). For Co, the same trend was observed (Figure 6b,d). Decrease in Co levels in tumor followed a gradual increase of the same element in spleen. For the Co–Fe NCs + HT group, the amount of Co in the spleen gradually increased from 2 to 3 μg on the first few days post-treatment to about 17 μg at 80 days post-treatment (Figure 6d). This low dose of Co could explain the absence of physical or psychological changes (i.e., no sufferings) in animals treated with Co–Fe NCs (no significant changes in weight was recorded throughout the course of this study; Figure S10, Supporting Information).

TEM micrographs of tumors, spleens, and livers of animals intratumorally injected with Co–Fe NCs showed evidence of nanocubes presence only at the tumor on day 10 and day 30 post-particle injection while no sign of nanocubes were observed in liver and spleen (Figures S11 and S12, Supporting Information). Remarkably, the size and shape of the Co–Fe NCs in the tumor at day 30 was different than that at day 10 and that of the original nanocubes themselves. In fact, measuring these morphological changes as a function of change in size and observed number of particles, we noticed significant differences in mean size (nm) and the total number of these deformed Co–Fe NCs on day 30 compared to day 10 (Figure S13, Supporting Information).

To verify the intrinsic toxicity of cobalt in Co–Fe NCs, an in vivo experiment was performed by replacing the cubic-shaped

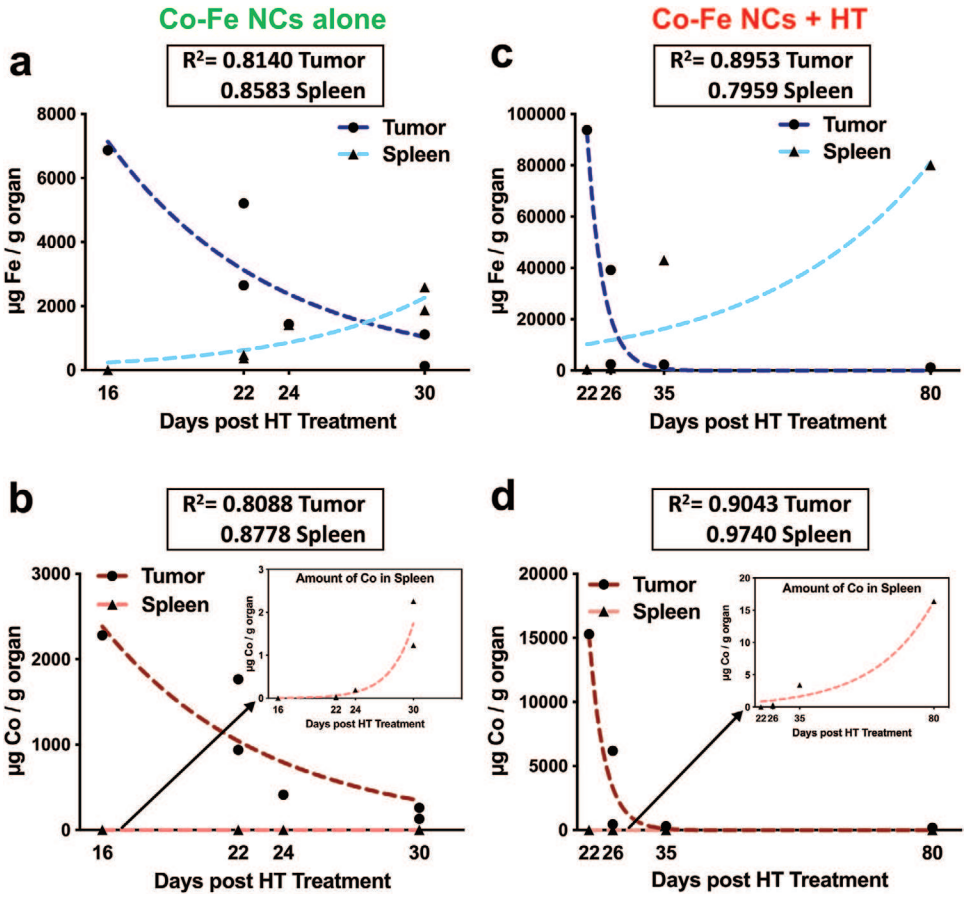

Figure 6. Profiling elimination of cobalt ferrite nanocubes at endpoint. a–d) ICP-MS elemental analysis of tumor and spleen post-treatment for Co–Fe NCs alone (a: Fe; b: Co) and Co–Fe NCs + HT (c: Fe; d: Co) showing consistent decrease of Fe and Co from tumor and simultaneous elimination of the same in spleen. The dashed lines represents a nonlinear (exponential) fit and respective R^2 values are listed above each graph.

Co–Fe NPs with an equivalent dose (single or multiple doses) of cobalt ions, injected i.t. in the form of a cobalt chloride ($CoCl_2$) salt (Figure S14, Supporting Information). Tumor growth showed no significant decrease compared to Control group, demonstrating that cobalt toxicity by itself cannot act as a potential monotherapy. Elemental analysis on day 20 of $CoCl_2$ injected animals showed majority of the Co ions in tumor (site of injection; 0.5 µg and 2.5 µg Co g^{-1} of tissue for single and multiple dose, respectively) and marginal increase (less than 0.5 µg Co g^{-1} of tissue) was seen at liver, kidney, and heart. No change in body weight of animals was seen proving tolerance toward injected $CoCl_2$ amounts (Figure S14, Supporting Information).

Overall, our study demonstrates that Co–Fe NCs can be used as an effective platform for a synergistic multimodal cancer therapy based on the magnetic hyperthermia in a nonconventional way. Indeed, the enhanced treatment outcome is due to multiple coexisting effects. First, Co–Fe NCs act as a mild hyperthermia agent, increasing the tumor temperature causing heat damage to the cancer cells. Second, the local injection helps maintain the Co–Fe NCs for a prolonged period within the tumor site, allowing for the gradually released cobalt to cause a slow yet potent toxicity against cancer cells. Indeed, the amphiphilic polymer coating enables the slow degradation of nanocubes within the tumor, preventing systemic toxicity during the elimination step. Third, we have demonstrated that only Co–Fe NCs tend to form chain-like structures, an effect that was further enhanced after HT. This phenomenon is observed for the first time at the tumor site in an in vivo study, that is further enhanced under an externally triggered remote magnetic source. Further, TEM analysis of the tumors showed that the AMF-induced chain formation was particular for Co–Fe NCs and not for IONCs. This result was further substantiated by a mathematical model suggesting that the large anisotropy of Co–Fe NCs renders them less susceptible to Néel relaxation than cubic shaped IONPs of similar size and shape, leading to stable magnetization states thus promoting the chain formation. In relation to the histology data demonstrating the movement of these particles from point of injection to the tumor periphery and combining it with visible chains in TEM images, we speculate that the collective migration of these chains under AMF could give rise to tumor reduction due to mechanical damage.

To enhance the toxic effects of Co–Fe NCs, other parameters may play key roles. For instance, a time lag (24–48 h) between Co–Fe NCs intratumoral injection and the time of application of HT treatment or the number of HT cycles to help grow the chain length further, can improve the synergy of the proposed multimodal therapy. The tuning of these parameters may help to reduce the dose of Co–Fe NCs, thus minimizing material side effects while maximizing therapeutic outcome. Further

investigations by testing these proposed parameters to improve the therapeutic outcome of this platform will be explored in future studies.

In conclusion, this study provides a new take on spinel mixed ferrites tailoring magnetic performance for biological application and encourages researchers to exploit both the intrinsic toxicity of included elements and unique unexplored physical mechanisms like chain formation under AMF, here observed, as a mean to provide tumor damage.

Experimental Section

Cell Culture: A431 epidermoid carcinoma cells (ATCC CRL-1555TM) were cultured using Dulbecco's modified Eagle medium (DMEM) media supplemented with 10% fetal bovine serum, 2% penicillin–streptavidin, and 1% L-glutamine (GibcoTM) under 37 °C, 5% CO_2, and 95% relative humidity.

Animal Model: Pathogen-free 8 week old female immunodeficient athymic NMRI nude mice, purchased from Charles River laboratories, were used for all the procedures. They were housed in IVC cages in a temperature-controlled room with a 12/12 h dark/light cycle, with ad libitum access to water and food. 1.5×10^6 A431 epidermoid carcinoma cells in 100 µL sterile saline were injected subcutaneously in the flank of each animal to induce the needed xenograft model. The tumor dimensions were recorded every alternate day using a caliper, and the tumor volumes were calculated using the formula: $V = Dd^2/2$, where D is the longest diameter of the tumor mass and d is the smallest diameter that is perpendicular to D. When the tumor volume reached ≈80–100 mm^3, the animals were distributed into different groups using a computer-generated randomization procedure. All animal experiments were performed in full compliance with Italian law d.lgs 116/92 (EU Directive 2010/63/EU for animal experiments) and the Istituto Italiano di Tecnologia (IIT) Ethical Committee. The animals' health and level of comfort were regularly checked by a veterinarian.

Short-Term Study Experiment Groups: The Control group ($N = 6$) was a group of untreated animals. The IONCs ($N = 6$) group was animals injected intratumorally with 50 µL of 14 g L^{-1} iron-oxide nanocubes (0.7 mg [Fe]/mice). The IONCs + HT ($N = 6$) group consisted of mice with tumor that was injected intratumorally with 50 µL of 14 g L^{-1} IONCs, and they were also subjected to 3 cycles of HT. The Co–Fe NCs ($N = 6$) group comprised animals that were injected intratumorally with 50 µL of 14 g L^{-1} cobalt ferrite nanocubes (0.7 mg [Fe + Co]/mice). The Co–Fe NCs + HT ($N = 6$) group consisted of animals that were injected intratumorally with 50 µL of Co–Fe NCs (0.7 mg [Fe + Co]/mice), and they were also subjected to 3 cycles of HT. During the tumor cell and particle injection procedures, the animals were anesthetized using a gas anesthesia system with isofluorane and oxygen mixture, and the tumors were immobilized using a sterile tweezer for a controlled intratumoral injection of the NPs. All the particle samples that were used for the in vivo experiments were prepared under sterile conditions, and they were UV-sterilized for 6 h prior to injection.

Long-Term Experiment Groups: Here, the amount of Co–Fe NCs injected intratumorally was manipulated according to individual tumor volume (0.7 mg NPs/80 mm^3 volume of tumor). The Control group ($N = 6$) consisted of animals with an untreated tumor (no particles or HT). The Co–Fe NCs ($N = 6$) group included mice injected intratumorally with Co–Fe NCs alone. The Co–Fe NCs + HT ($N = 6$) group comprised animals injected intratumorally with Co–Fe NCs, and then subjected to 3 cycles of HT. During the particle injection procedures, the animals were anesthetized using gas anesthesia (isoflurane and oxygen mix), and the tumors were immobilized using a sterile tweezer for a controlled injection of the NPs within the tumor.

Hyperthermia Therapy and Temperature Monitoring: 5 min after the NPs were injected, in both short- and long-term experiments, the animals in group with HT were subjected to AMF, which was generated by a MagneTerm AC system (Nanotherics, Corp), for 30 min (HT1). The animals were then subjected to two more cycles of HT, each of which lasted 30 min (HT2 and HT3), over the next 2 days. The field and frequency of the AMF used was 20 kA m^{-1} and 110 kHz, respectively. During the course of HT, the animals were anesthetized using intraperitoneal injection of ketamine/xylazine mixture prepared by the inhouse veterinarian that lasted for 30–40 min (course of HT treatments). The temperature of the mouse's skin and tumor was monitored using an IR camera (Fluka, Inc.) throughout the course of HT therapy. All the images were processed by Fluka Software, which was provided by the manufacturer. The animals experiencing HT treatments were observed under IR lamp until they regained consciousness and mobility and then moved to their respective cages.

Endpoints: All animals were sacrificed in a humane manner 12 days postparticle injection and HT1 in the case of the short-term experiment. The humane endpoint for the long-term experiment was when at least one diameter of the tumor reached 2 cm in length (NIH guidelines).

Statistics: For LDH assay (Figure 1d), 2-way analysis of variance (ANOVA) using Tukey's multiple comparison test was used to analyze significance between each group at different time points. Statistical significance for tumor growth curve analysis (Figure 5c) was calculated using one-way ANOVA (Tukey's multiple comparison test). P value was 0.0023 and 0.0004 between CTRL and Co–Fe NCs, CTRL, and Co–Fe NCs + HT, respectively. Statistical significance for survival study (Figure 5d) was calculated using log-rank (Mantel–Cox) test. P value was 0.0367 and 0.0033 between CTRL and Co–Fe NCs, CTRL, and Co–Fe NCs + HT, respectively. P values were calculated using Prism GraphPad, GP: 0.1234 (ns), 0.0332 (*), 0.0021 (**), 0.0002 (***), and <0.0001 (****).

Supporting Information

Supporting Information is available from the Wiley Online Library or from the author.

Acknowledgements

This work was partially funded by the European Research Council (starting grant ICARO, Contract No. 678109) and partially by the AIRC project (Contract No. 14527). The authors also acknowledge Centro de Supercomputación de Galicia (CESGA) for the computational resources. D.S. acknowledges Xunta de Galicia for financial support under the I2C Plan and the Strategic Grouping in Materials (AeMAT; Grant No. ED431E2018/08). This work made use of computational facilities funded by the Small items of research equipment at the University of York ENERGY (Grant No. EP/K031589/1). All animal experimental protocols were in full compliance with Italian law d.lgs 116/92 (EU Directive 2010/63/EU for animal experiments) and the Istituto Italiano di Tecnologia (IIT) Ethical Committee. The animals' health and level of comfort were regularly checked by a veterinarian. The authors acknowledge Dr. Tiziano Catelani for assistance with sample preparation for TEM observation at the TEM facility at Istituto Italiano di Tecnologia, Genova, Italy.

Conflict of Interest

The authors declare no conflict of interest.

Keywords

cancer therapy, cobalt ferrite nanoparticles, cobalt toxicity, magnetic hyperthermia, particle alignment

Received: May 31, 2020
Revised: July 23, 2020
Published online:

[1] K. Maier-Hauff, F. Ulrich, D. Nestler, H. Niehoff, P. Wust, B. Thiesen, H. Orawa, V. Budach, A. Jordan, *J. Neuro-Oncol.* **2011**, *103*, 317.
[2] C. Martinez-Boubeta, K. Simeonidis, A. Makridis, M. Angelakeris, O. Iglesias, P. Guardia, A. Cabot, L. Yedra, S. Estradé, F. Peiró, Z. Saghi, P. A. Midgley, I. Conde-Leborán, D. Serantes, D. Baldomir, *Sci. Rep.* **2013**, *3*, 1652.
[3] a) P. Guardia, A. Riedinger, S. Nitti, G. Pugliese, S. Marras, A. Genovese, M. E. Materia, C. Lefevre, L. Manna, T. Pellegrino, *J. Mater. Chem. B* **2014**, *2*, 4426; b) P. Guardia, R. Di Corato, L. Lartigue, C. Wilhelm, A. Espinosa, M. Garcia-Hernandez, F. Gazeau, L. Manna, T. Pellegrino, *ACS Nano* **2012**, *6*, 3080.
[4] S.-H. Noh, W. Na, J.-T. Jang, J.-H. Lee, E. J. Lee, S. H. Moon, Y. Lim, J.-S. Shin, J. Cheon, *Nano Lett.* **2012**, *12*, 3716.
[5] A. Sathya, P. Guardia, R. Brescia, N. Silvestri, G. Pugliese, S. Nitti, L. Manna, T. Pellegrino, *Chem. Mater.* **2016**, *28*, 1769.
[6] D. Carta, M. F. Casula, A. Falqui, D. Loche, G. Mountjoy, C. Sangregorio, A. Corrias, *J. Phys. Chem. C* **2009**, *113*, 8606.
[7] J. Carrey, B. Mehdaoui, M. Respaud, *J. Appl. Phys.* **2011**, *109*, 083921.
[8] a) A. Espinosa, R. Di Corato, J. Kolosnjaj-Tabi, P. Flaud, T. Pellegrino, C. Wilhelm, *ACS Nano* **2016**, *10*, 2436; b) A. K. Hauser, M. I. Mitov, E. F. Daley, R. C. McGarry, K. W. Anderson, J. Z. Hilt, *Biomaterials* **2016**, *105*, 127; c) S. Kossatz, J. Grandke, P. Couleaud, A. Latorre, A. Aires, K. Crosbie-Staunton, R. Ludwig, H. Dähring, V. Ettelt, A. Lazaro-Carrillo, M. Calero, M. Sader, J. Courty, Y. Volkov, A. Prina-Mello, A. Villanueva, Á. Somoza, A. L. Cortajarena, R. Miranda, I. Hilger, *Breast Cancer Res.* **2015**, *17*, 66; d) S. A. Meenach, C. G. Otu, K. W. Anderson, J. Z. Hilt, *Int. J. Pharm.* **2012**, *427*, 177.
[9] B. T. Mai, P. B. Balakrishnan, M. J. Barthel, F. Piccardi, D. Niculaes, F. Marinaro, S. Fernandes, A. Curcio, H. Kakwere, G. Autret, R. Cingolani, F. Gazeau, T. Pellegrino, *ACS Appl. Mater. Interfaces* **2019**, *11*, 5727.
[10] J. Kolosnjaj-Tabi, R. Di Corato, L. Lartigue, I. Marangon, P. Guardia, A. K. A. Silva, N. Luciani, O. Clément, P. Flaud, J. V. Singh, P. Decuzzi, T. Pellegrino, C. Wilhelm, F. Gazeau, *ACS Nano* **2014**, *8*, 4268.
[11] a) S. Amiri, H. Shokrollahi, *Mater. Sci. Eng., C* **2013**, *33*, 1; b) E. Mazario, N. Menéndez, P. Herrasti, M. Cañete, V. Connord, J. Carrey, *J. Phys. Chem. C* **2013**, *117*, 11405; c) Q. Song, Z. J. Zhang, *J. Am. Chem. Soc.* **2004**, *126*, 6164; d) L. Horev-Azaria, G. Baldi, D. Beno, D. Bonacchi, U. Golla-Schindler, J. C. Kirkpatrick, S. Kolle, R. Landsiedel, O. Maimon, P. N. Marche, J. Ponti, R. Romano, F. Rossi, D. Sommer, C. Uboldi, R. E. Unger, C. Villiers, R. Korenstein, *Part. Fibre Toxicol.* **2013**, *10*, 32; e) R. Wan, Y. Mo, Z. Zhang, M. Jiang, S. Tang, Q. Zhang, *Part. Fibre Toxicol.* **2017**, *14*, 38; f) D. W. Hwang, D. S. Lee, S. Kim, *Soc. Nucl. Med.* **2012**, *53*, 106; g) F. Finetti, E. Terzuoli, S. Donnini, M. Uva, M. Ziche, L. Morbidelli, *PLoS One* **2016**, *11*, e0168727.
[12] H. A. Albarqi, L. H. Wong, C. Schumann, F. Y. Sabei, T. Korzun, X. Li, M. N. Hansen, P. Dhagat, A. S. Moses, O. Taratula, O. Taratula, *ACS Nano* **2019**, *13*, 6383.
[13] J. H. Lee, J. T. Jang, J. S. Choi, S. H. Moon, S. H. Noh, J. W. Kim, J. G. Kim, I. S. Kim, K. I. Park, J. Cheon, *Nat. Nanotechnol.* **2011**, *6*, 418.
[14] D. Psimadas, G. Baldi, C. Ravagli, P. Bouziotis, S. Xanthopoulos, M. C. Franchini, P. Georgoulias, G. Loudos, *J. Biomed. Nanotechnol.* **2012**, *8*, 575.
[15] J. I. Kim, C. Chun, B. Kim, J. M. Hong, J.-K. Cho, S. H. Lee, S.-C. Song, *Biomaterials* **2012**, *33*, 218.
[16] a) E. Aşık, Y. Akpınar, N. T. Güray, M. İşcan, G. Ç. Demircigil, M. Volkan, *Toxicol. Res.* **2016**, *5*, 1649; b) V. B. Bregar, J. Lojk, V. Suštar, P. Veranič, M. Pavlin, *Int. J. Nanomed.* **2013**, *8*, 919; c) J. Kolosnjaj-Tabi, L. Lartigue, Y. Javed, N. Luciani, T. Pellegrino, C. Wilhelm, D. Alloyeau, F. Gazeau, *Nano Today* **2016**, *11*, 280.
[17] J. Volatron, J. Kolosnjaj-Tabi, Y. Javed, Q. L. Vuong, Y. Gossuin, S. Neveu, N. Luciani, M. Hemadi, F. Carn, D. Alloyeau, F. Gazeau, *Sci. Rep.* **2017**, *7*, 40075.
[18] a) B. Desoize, *Anticancer Res.* **2004**, *24*, 1529; b) S. Dasari, P. B. Tchounwou, *Eur. J. Pharmacol.* **2014**, *740*, 364.
[19] a) L. Balcells, I. Stankovic, Z. Konstantinovic, A. Alagh, V. Fuentes, L. Lopez-Mir, J. Oro, N. Mestres, C. Garcia, A. Pomar, B. Martinez, *Nanoscale* **2019**, *11*, 14194; b) R. J. Wilson, W. Hu, C. W. P. Fu, A. L. Koh, R. S. Gaster, C. M. Earhart, A. Fu, S. C. Heilshorn, R. Sinclair, S. X. Wang, *J. Magn. Magn. Mater.* **2009**, *321*, 1452; c) G. Cheng, D. Romero, G. T. Fraser, A. R. Hight Walker, *Langmuir* **2005**, *21*, 12055.
[20] a) R. Di Corato, A. Quarta, P. Piacenza, A. Ragusa, A. Figuerola, R. Buonsanti, R. Cingolani, L. Manna, T. Pellegrino, *J. Mater. Chem.* **2008**, *18*, 1991; b) T. Pellegrino, L. Manna, S. Kudera, T. Liedl, D. Koktysh, A. L. Rogach, S. Keller, J. Rädler, G. Natile, W. J. Parak, *Nano Lett.* **2004**, *4*, 703.
[21] R. Hergt, S. Dutz, R. Müller, M. Zeisberger, *J. Phys.: Condens. Matter* **2006**, *18*, S2919.
[22] V. Pašukonienė, A. Mlynska, S. Steponkienė, V. Poderys, M. Matulionytė, V. Karabanovas, U. Statkutė, R. Purvinienė, J. A. Kraśko, A. Jagminas, M. Kurtinaitienė, M. Strioga, R. Rotomskis, *Medicina* **2014**, *50*, 237.
[23] a) R. Di Corato, A. Espinosa, L. Lartigue, M. Tharaud, S. Chat, T. Pellegrino, C. Ménager, F. Gazeau, C. Wilhelm, *Biomaterials* **2014**, *35*, 6400; b) M. V. Zyuzin, M. Cassani, M. J. Barthel, H. Gavilan, N. Silvestri, A. Escudero, A. Scarpellini, F. Lucchesi, F. J. Teran, W. J. Parak, T. Pellegrino, *ACS Appl. Mater. Interfaces* **2019**, *11*, 41957.
[24] a) D. Cabrera, A. Lak, T. Yoshida, M. E. Materia, D. Ortega, F. Ludwig, P. Guardia, A. Sathya, T. Pellegrino, F. J. Teran, *Nanoscale* **2017**, *9*, 5094; b) G. Salas, J. Camarero, D. Cabrera, H. Takacs, M. Varela, R. Ludwig, H. Dähring, I. Hilger, R. Miranda, M. d. P. Morales, F. J. Teran, *J. Phys. Chem. C* **2014**, *118*, 19985; c) J.-P. Fortin, C. Wilhelm, J. Servais, C. Ménager, J.-C. Bacri, F. Gazeau, *J. Am. Chem. Soc.* **2007**, *129*, 2628.
[25] R. E. Rosensweig, *J. Magn. Magn. Mater.* **2002**, *252*, 370.
[26] a) D. Serantes, K. Simeonidis, M. Angelakeris, O. Chubykalo-Fesenko, M. Marciello, M. d. P. Morales, D. Baldomir, C. Martinez-Boubeta, *J. Phys. Chem. C* **2014**, *118*, 5927; b) A. M. Huízar-Félix, D. Muñoz, I. Orue, C. Magén, A. Ibarra, J. M. Barandiarán, A. Muela, M. L. Fdez-Gubieda, *Appl. Phys. Lett.* **2016**, *108*, 063109.
[27] I. Marangon, A. A. K. Silva, T. Guilbert, J. Kolosnjaj-Tabi, C. Marchiol, S. Natkhunarajah, F. Chamming's, C. Ménard-Moyon, A. Bianco, J.-L. Gennisson, G. Renault, F. Gazeau, *Theranostics* **2017**, *7*, 329.
[28] X.-Y. Chu, W. Huang, Y.-L. Wang, L.-W. Meng, L.-Q. Chen, M.-J. Jin, L. Chen, C.-H. Gao, C. Ge, Z.-G. Gao, C.-S. Gao, *Int. J. Nanomed.* **2019**, *14*, 689.
[29] a) J. Kolosnjaj-Tabi, Y. Javed, L. Lartigue, J. Volatron, D. Elgrabli, I. Marangon, G. Pugliese, B. Caron, A. Figuerola, N. Luciani, T. Pellegrino, D. Alloyeau, F. Gazeau, *ACS Nano* **2015**, *9*, 7925; b) M. Levy, N. Luciani, D. Alloyeau, D. Elgrabli, V. Deveaux, C. Pechoux, S. Chat, G. Wang, N. Vats, F. Gendron, C. Factor, S. Lotersztajn, A. Luciani, C. Wilhelm, F. Gazeau, *Biomaterials* **2011**, *32*, 3988.